

Asteroseismic modelling of the metal-poor star τ Ceti

Y. K. Tang^{1,2} and N. Gai^{3,4}

¹ Department of Physics, Dezhou University, Dezhou 253023, P. R. China
e-mail: tyk450@163.com

² Key Lab of Biophysics in Universities of Shandong, Dezhou 253023, P. R. China

³ Department of Astronomy, Beijing Normal University, Beijing 100875, P. R. China
e-mail: gaining@mail.bnu.edu.cn

⁴ Department of Astronomy, Yale University, P.O. Box 208101, New Haven, CT 06520-8101, USA

Preprint online version: August 15, 2018

ABSTRACT

Context. Asteroseismology is an efficient tool not only for testing stellar structure and evolutionary theory but also constraining the parameters of stars for which solar-like oscillations are detected, presently. As an important southern asteroseismic target, τ Ceti, is a metal-poor star. The main features of the oscillations and some frequencies of τ Ceti have been identified. Many scientists propose to comprehensively observe this star as part of the Stellar Observations Network Group.

Aims. Our goal is to obtain the optimal model and reliable fundamental parameters for the metal-poor star τ Ceti by combining all non-asteroseismic observations with these seismological data.

Methods. Using the Yale stellar evolution code (YREC), a grid of stellar model candidates that fall within all the error boxes in the HR diagram have been constructed, and both the model frequencies and large- and small- frequency separations are calculated using the Guenther's stellar pulsation code. The $\chi^2_{\nu c}$ minimization is performed to identify the optimal modelling parameters that reproduce the observations within their errors. The frequency corrections of near-surface effects to the calculated frequencies using the empirical law, as proposed by Kjeldsen and coworkers, are applied to the models.

Results. We derive optimal models, corresponding to masses of about $0.775 - 0.785 M_{\odot}$ and ages of about 8 – 10 Gyr. Furthermore, we find that the quantities derived from the non-asteroseismic observations (effective temperature and luminosity) acquired spectroscopically are more accurate than those inferred from interferometry for τ Ceti, because our optimal models are in the error boxes B and C, which are derived from spectroscopy results.

Key words. stars: Asteroseismology – Stars: evolution – Stars: individual: τ Ceti

1. Introduction

The solar five-minute oscillations have led to a wealth of information about the internal structure of the Sun. These results have stimulated various attempts to detect solar-like oscillations for a handful of solar-type stars. Solar-like oscillations have been confirmed for several main-sequence, subgiant and red giant stars by the ground-based observations or by the CoRoT and the Kepler space missions, such as ν Indi (Bedding et al. 2006; Carrier et al. 2007), α Cen A (Bouchy & Carrier 2002; Bedding et al. 2004), α Cen B (Carrier & Bourban 2003a; Kjeldsen et al. 2005), μ Arae (Bouchy et al. 2005), HD 49933 (Mosser et al. 2005), β Vir (Martić et al. 2004a; Carrier et al. 2005a), Procyon A (Martić et al. 2004b; Eggenberger et al. 2004a; Arentoft et al. 2008; Bedding et al. 2010), η Bootis (Kjeldsen et al. 2003; Carrier et al. 2005b), β Hyi (Bedding et al. 2001, 2007; Carrier et al. 2001), δ Eri (Carrier et al. 2003b), 70 Ophiuchi A (Carrier & Eggenberger 2006), ϵ Oph (Ridder et al. 2006), CoRoT target HR7349 (Carrier et al. 2010), KIC 6603624, KIC 3656476 and KIC 11026764 (Chaplin et al. 2010), etc. Furthermore, the large and small frequency separations of p-modes can provide a good estimate of the mean density and age of the stars (Ulrich 1986, 1988). On the basis of these asteroseismic data, numerous theoretical analyses have been performed to determine precise global stellar parameters and test the various complicate physical effects on the stellar structure and evolutionary theory (Thévenin

et al. 2002; Eggenberger et al. 2004b, 2005; Kervella et al. 2004; Miglio & Montalbán 2005; Provost et al. 2004, 2006; Tang et al. 2008a, 2008b).

τ Ceti (HR 509, HD 10700) is a G8 V metal-poor star, belonging to population II. Extensive analyse of this star have been performed by many scientists who have provided different non-seismic observational results (such as effective temperature T_{eff} and luminosity L), depending on the different methods used, i.e. interferometry and spectroscopy. Teixeira et al. (2009) detected solar-like oscillations on τ Ceti, identified some possible existing frequencies, and obtained the large separation around $\Delta\nu = 169 \mu\text{Hz}$ with HARPS. These seismological data will provide a constraint on the fundamental parameters of τ Ceti. Moreover, τ Ceti will be one of the most promising southern asteroseismic targets of the seismology programme of Stellar Observations Network Group (Metcalfe et al. 2010).

In this work, using a mixture of conventional and asteroseismic observed constraints, we try to determine modelling parameters of τ Ceti with YREC. The observational constraints available to τ Ceti are summarized in Sect. 2, while the details of the evolutionary models are presented in Sect. 3. The seismic analyses are carried out in Sect. 4. Finally, the discussion and conclusions are given in Sect. 5.

Table 1. Non-asteroseismic observational data of τ Ceti.

| Observable | Value | Source |
|-------------------------------------------|---------------------|--------|
| Effective temperature T_{eff} (K) | 5264 ± 100 | (1) |
| | 5525 ± 12 | (3) |
| Luminosity L/L_{\odot} | 0.52 ± 0.03 | (4) |
| | 0.50 ± 0.006 | (3) |
| | 0.488 ± 0.010 | (2) |
| Metallicity $[Fe/H]_s$ | -0.5 ± 0.03 | (1) |
| Surface heavy-element abundance $[Z/X]_s$ | 0.0073 ± 0.0005 | (5) |
| | 0.773 ± 0.024 | (5) |

References.—(1) Soubiran et al. (1998), (2) Teixeira et al. (2009), (3) Pijpers et al. (2003a), (4) Pijpers (2003b), (5) this paper.

2. Observational constraints

2.1. Non-asteroseismic observational constraints

The metallicity derived from observations is $[Fe/H] = -0.5 \pm 0.03$ (Soubiran et al. 1998). The mass fraction of heavy-elements, Z , was derived assuming $\log[Z/X] \approx [Fe/H] + \log[Z/X]_{\odot}$, and $[Z/X]_{\odot} = 0.0230$ (Grevesse and Sauval, 1998), for the solar mixture. We can therefore deduce that $[Z/X]_s = 0.0068 - 0.0078$. The radius, as an important parameter for constraining stellar models, was first measured by Pijpers et al. (2003a) using interferometry. They determined the radius of τ Ceti corresponding to $0.773 \pm 0.004_{(int.)} \pm 0.02_{(ext.)} R_{\odot}$. The measurement of the radius was then improved by Di Folco et al. (2004) and Di Folco et al. (2007). Finally, Di Folco et al. (2007) determined the radius $R = 0.790 \pm 0.005 R_{\odot}$. In our work, we use a large value of radius $R = 0.773 \pm 0.024 R_{\odot}$ which includes all the surrounding observational radius.

The effective temperature and luminosity of τ Ceti are both derived from spectroscopy (5264 ± 100 K and $0.52 \pm 0.03 L_{\odot}$), and by ensuring that we reproduce the measured radius (5525 ± 12 K, $0.500 \pm 0.006 L_{\odot}$), using interferometry (Soubiran et al. 1998; Pijpers et al. 2003a, 2003b). In addition the luminosity of a star can be obtained by combining our knowledge of the magnitude and distance. For τ Ceti, the apparent magnitude $V = 3.50 \pm 0.01$, with the revised parallax, gives an absolute magnitude $M_V = 5.69 \pm 0.01$. Teixeira et al. (2009) derived a luminosity for τ Ceti of $L/L_{\odot} = 0.488 \pm 0.010$, using bolometric correction for τ Ceti $B.C. = -0.17 \pm 0.02$ (Casagrande et al. 2006) and adopting an absolute bolometric magnitude for the Sun of $M_{bol,\odot} = 4.74$ (Bessel et al. 1998).

Using above different effective temperatures and luminosities, we can obtain three error boxes, which error box A (5525 ± 12 K, $0.50 \pm 0.006 L_{\odot}$) are denoted by crosses, error box B (5264 ± 100 K, $0.52 \pm 0.03 L_{\odot}$) denoted by triangles, and error box C (5264 ± 100 K, $0.488 \pm 0.010 L_{\odot}$) denoted by diamonds, shown in Fig. 1(d), respectively. Meanwhile, we decided to increase all errors by a factor of 1.5, so that our calibration of the star is only weakly constrained by these values.

All non-asteroseismic observational constraints are listed in Table 1.

2.2. Asteroseismic constraints

Solar-like oscillations of the G8V star τ Ceti were detected by Teixeira et al. (2009) with the HARPS spectrograph. Thirty-one individual modes are identified (see Table 1 in Teixeira et al. 2009). The large frequency separation is about $\Delta\nu = 169 \mu\text{Hz}$.

Table 2. Input parameters for model tracks.

| Variable | Minimum | Maximum | δ |
|---------------------------------------|---------|---------|----------|
| | Value | Value | |
| Mass M/M_{\odot} | 0.770 | 0.795 | 0.005 |
| Mixing length α | 0.8 | 1.8 | 0.2 |
| Initial heavy element abundance Z_i | 0.001 | 0.008 | 0.0005 |
| Initial hydrogen abundance X_i | 0.70 | 0.75 | 0.01 |

Note.—The value δ defines the increment between minimum and maximum parameter values used to create the model array.

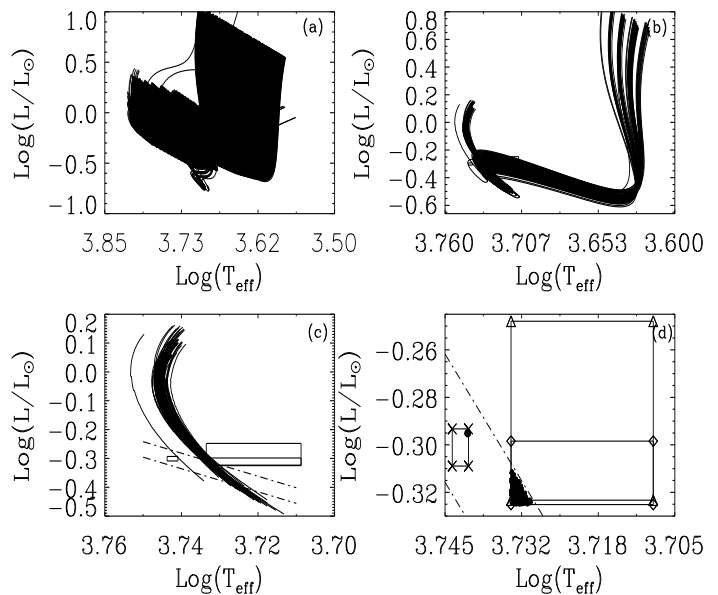


Fig. 1. (a) All evolutionary tracks in the HR diagram; (b) Evolutionary tracks falling in the error boxes from pre-main sequence to main sequence; (c) Blow up the evolutionary tracks falling in the error boxes in the main sequence; (d) The selected models falling in the error boxes. Error box A (5525 ± 12 K, $0.50 \pm 0.006 L_{\odot}$) is denoted by crosses, error box B (5264 ± 100 K, $0.52 \pm 0.03 L_{\odot}$) denoted by triangles, and error box C (5264 ± 100 K, $0.488 \pm 0.010 L_{\odot}$) denoted by diamonds, respectively.

3. Stellar models

We calculated many evolutionary tracks using Yale stellar evolution code (YREC; Demarque et al. 2008) by inputting different parameters shown in Table 2.

The mass range are $M = 0.770 - 0.795 M_{\odot}$ with the increment value $0.005 M_{\odot}$. Initial heavy element abundance range are Z_i ($0.001 - 0.008$) with the increment value 0.0005 and initial hydrogen abundance X_i ($0.70 - 0.75$) with the increment value 0.01 . Energy transfer by convection is treated according to the standard mixing-length theory, and the boundaries of the convection zones are determined by the Schwarzschild criterion (see Demarque et al. 2008 for details of the YREC). We set the mixing length parameter $\alpha = 0.8 - 1.8$ with the increment value 0.2 . Using these parameter space, we created the model array. The initial zero-age main sequence (ZAMS) model used for τ Ceti is created from pre-main-sequence evolution calculations. These models are calculated using the updated OPAL equation-of-state tables EOS2005 (Rogers and Nayfonov, 2002). We used OPAL high temperature opacities (Iglesias and Rogers 1996) supplemented with low temperature opacities from Ferguson et al.

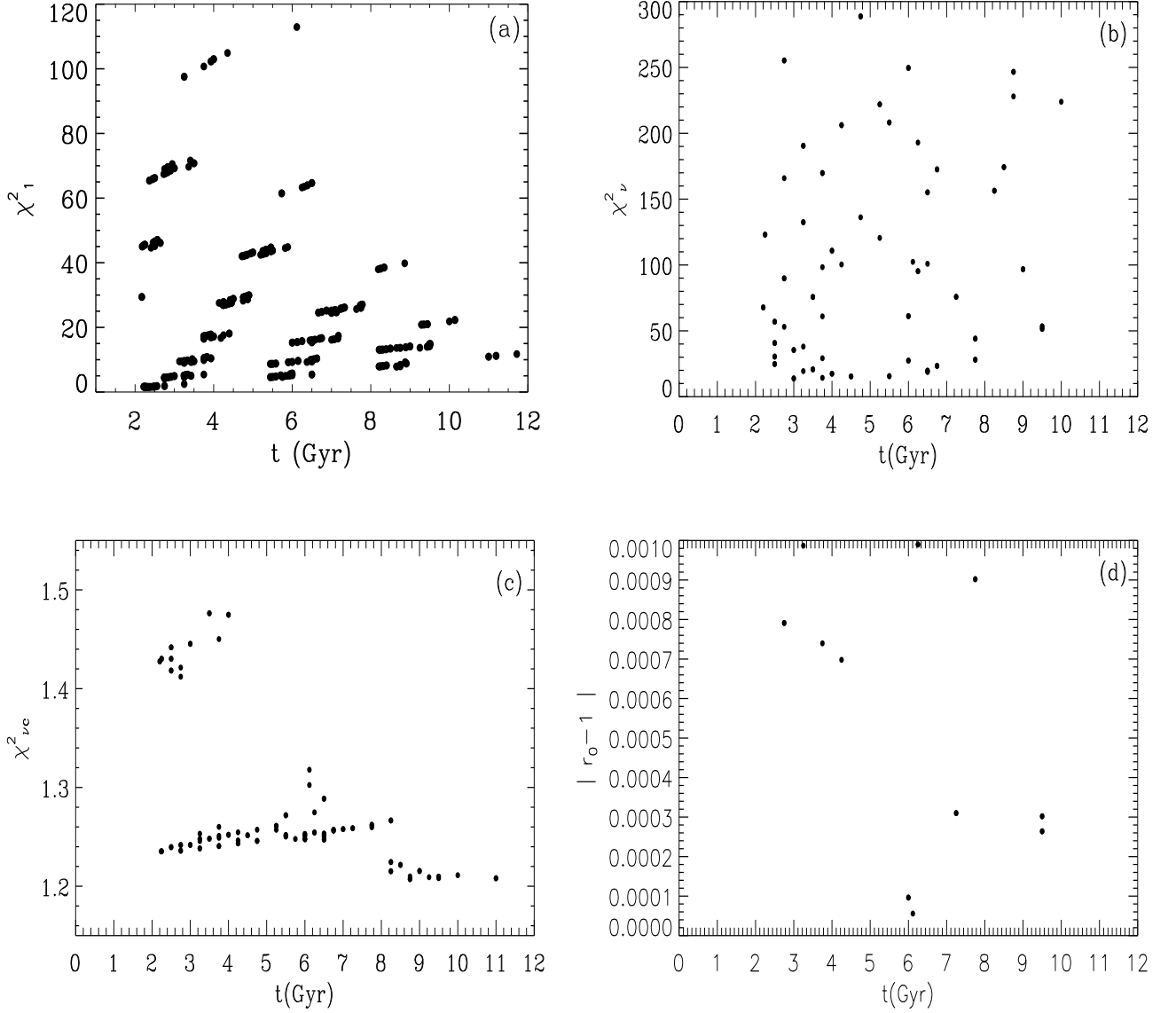


Fig. 2. (a) χ^2_1 values derived from Eq.(2), plotted as a function of age; (b) χ^2_ν values derived from Eq.(3), plotted as a function of age; (c) χ^2_{vc} values derived from Eq.(6), plotted as a function of age; (d) $|r_0 - 1|$ values plotted as a function of age.

(2005). The NACRE nuclear reaction rates (Angulo et al. 1999) were used. The Krishna-Swamy Atmosphere T- τ relation is used for solar-like star (Guenther and Demarque 2000). All models included gravitational settling of helium and heavy elements using the formulation of Thoul et al. (1994).

Figure 1(a) shows that many evolutionary tracks cover all possible evolutionary status of τ Ceti. According to the above four error boxes, we select all the tracks crossing the error boxes shown in Fig. 1(b). We only choose to study main-sequence models, which are shown in Fig. 1(c). Meanwhile, we use the mass and radius to estimate the large separation according to Eq. (1) (Kjeldsen & Bedding 1995; Miglio et al. 2009). Furthermore, using the temperature, luminosity, radius, and larger separation (refer to the values from Teixeira et al. 2009) as constraint, we select the models of τ Ceti provided in Fig. 1(d) as candidates.

$$\Delta\nu = \sqrt{\frac{M/M_\odot}{(R/R_\odot)^3}} \times 134.9 \mu\text{Hz} \quad (1)$$

We now consider a function that describes the agreement between the observations and the theoretical results

$$\chi^2_1 = \frac{1}{5} \sum_{i=1}^5 \left(\frac{C_i^{theo} - C_i^{obs}}{\sigma C_i^{obs}} \right)^2, \quad (2)$$

where \mathbf{C} represents the quantities L/L_\odot , T_{eff} , R/R_\odot , and $[Fe/H]_s$ and large frequency separation $\Delta\nu$, \mathbf{C}^{theo} represents the theoretical values, and \mathbf{C}^{obs} represents the observational values listed in Table 1. The vector $\sigma \mathbf{C}_i^{obs}$ contain the errors in these observations, which are also given in Table 1. We also decided to adopt a large error (all errors are increased by a factor of 1.5), so that our calibration of the star is only weakly constrained by these values, which is not precisely determined. Figure 2(a)

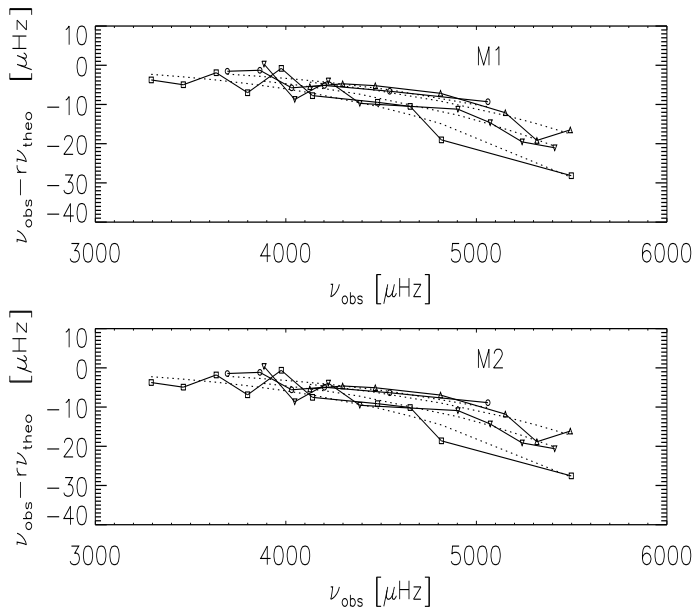


Fig. 3. The difference between observed and best-fit model frequencies, according to the left term of Eq.(4). Squares are used for $l = 0$ modes, diamonds for $l = 1$ modes, triangles for $l = 2$ modes, and circles for $l = 3$. Dotted lines show the power-law function, according to the right term of Eq.(4).

presents the values χ_1^2 versus age t of selected models that are shown in Fig.1(d). We find that we cannot select an optimal model from Fig.2(a). From Fig.2(a), we find that it is difficult to select an optimal model depending mainly on the non-seismic constraints and $\Delta\nu$, which was estimated by simply scaling from solar value using Eq.(1). Hence, a detailed pulsation analysis are needed in the next step.

4. Asteroseismic constraints of fundamental parameters

Using Guenther's pulsation code (Guenther 1994), we calculate the adiabatic low- l p -mode frequencies, the large- and small- frequency separations ($\Delta\nu_{n,l} \equiv \nu_{n,l} - \nu_{n-1,l}$ and $\delta\nu_{n,l} \equiv \nu_{n,l} - \nu_{n-1,l+2}$, defined by Tassoul 1980) of all the selected models. We compare the theoretical frequencies with the corresponding observational frequencies using the function χ_v^2

$$\chi_v^2 = \frac{1}{N} \sum_{n,l} \left(\frac{\nu_l^{theo}(n) - \nu_l^{obs}(n)}{\sigma} \right)^2, \quad (3)$$

where, $N=31$ is the total number of modes, and $\nu_l^{theo}(n)$ and $\nu_l^{obs}(n)$ are the theoretical and observed frequencies respectively, for each spherical degree l and the radial order n , where $\sigma = 2\mu\text{Hz}$ (Teixeira et al. 2009) represents the uncertainty in the observed frequencies and χ_v^2 values, plotted as function of age, are shown in Fig.2(b).

Since existing stellar models fail to accurately represent the near-surface layers of the solar-like stars, where the turbulent convection take place, the systematic offset between the observed and model frequencies appears. Furthermore, this offset between observed and best model frequencies turns out to be closely fitted by a power law (Christensen-Dalsgaard & Gough 1980; Kjeldsen et al. 2008; Metcalfe et al. 2009; Doğan et al. 2009, 2010; Bedding et al. 2010; Christensen-Dalsgaard et al.

2010). In other words, this offset increases with increasing frequency shown in Fig.3. This power law can be expressed using the equation

$$\nu_{obs}(n) - r_l \nu_{theo}(n) = a_l [\nu_{obs}(n_i) / \nu_{max}]^b, \quad (4)$$

where ν_{obs} are the observed frequencies of radial and non-radial order, $\nu_{best} = r_l \nu_{theo}(n)$ are the corresponding calculated frequencies of the best-fit model, and ν_{max} is a constant frequency corresponding to the peak power in the spectrum, which is taken as $4490 \mu\text{Hz}$ for τ Ceti and r_l , a_l , and b are parameters described in detail by Kjeldsen et al. (2008), (For a different spherical degree l , the values of r and a are denoted by r_l and a_l , respectively.). For the Sun and a solar-like star, the exponent $b = 4.90$ is appropriate, as has been proven by many scientists. We use the Kjeldsen et al. (2008) prescription to correct the theoretical frequencies from near surface effects.

According to Eq. (4), we can use the following equation to obtain the corrected frequencies of models:

$$\nu_{correct}(n) = r_l \nu_{theo}(n) + a_l [\nu_{obs}(n) / \nu_{max}]^b. \quad (5)$$

We define the function χ_{vc}^2 in a similar way to Eq.(3) as

$$\chi_{vc}^2 = \frac{1}{N} \sum_{n,l} \left(\frac{\nu_l^{correct}(n) - \nu_l^{obs}(n)}{\sigma(\nu_l^{obs}(n))} \right)^2. \quad (6)$$

The values of χ_{vc}^2 , plotted as a function of age are shown in Fig.2(c). From Fig. 2(c), we can see that the values of χ_{vc}^2 are lower than χ_v^2 and their lowest values correspond to model ages from 8 to 10 Gyr. We conclude that the optimal model corresponds to the lower values of χ_v^2 and $r_0 - 1$. From Figs.2(c) and 2(d), we infer that only two models M1 and M2 can be accurately described by the observational constraints. The difference between the observed and uncorrected model frequencies of M1 and M2 are shown in Fig. 3. The uncorrected and corrected frequencies of the optimal models M1 and M2 and the observational frequencies are shown in Table 3.

To clearly compare all of the theoretical frequencies of the models with observational frequencies, we provide echelle diagrams of models M1 and M2 in Fig.4. An Echelle diagram is a useful tool for comparing stellar models with observations. This diagram presents the mode frequencies along the ordinate axis, and the same frequencies modulo the large separations in abscissae. From Figs.4(a) and 4(d), it can be seen that the uncorrected theoretical frequencies are not closely in agreement with the observed frequencies. The corrected theoretical frequencies indicated by Eq. (5) fit perfectly the observation shown in Figs.4(b) and 4(e). Because the observed frequencies of orders n are not consecutive and the values of $\nu_{obs}(n)$ are very close to those of $\nu_{theo}(n)$, we substitute the $\nu_{theo}(n) / \nu_{max}$ for $\nu_{obs}(n) / \nu_{max}$. Hence Eq. (5) becomes

$$\nu_{correct}(n) = r \nu_{theo}(n) + a [\nu_{theo}(n) / \nu_{max}]^b. \quad (7)$$

From Figs.4(b), 4(c), 4(e), and 4(f), it can be seen that corrected frequencies given by Eq. (5) and (7) respectively are uniform and reproduce the observed frequencies perfectly. Furthermore, we can use the function χ_{vc}^2 to select the fitting model parameters. As we all know, the suitable model parameters correspond to the lowest values of χ_{vc}^2 , which can be clearly seen in Fig. 5. From Fig. 5, we can conclude that the mass is in the range $0.775 - 0.785 M_\odot$, α is in the range $1.6 - 1.8$, Z_i in $0.0065 - 0.0075$, and X_i $0.73 - 0.75$. Hence, the model parameters of τ Ceti can be constrained to within these narrow ranges. Finally, we list the

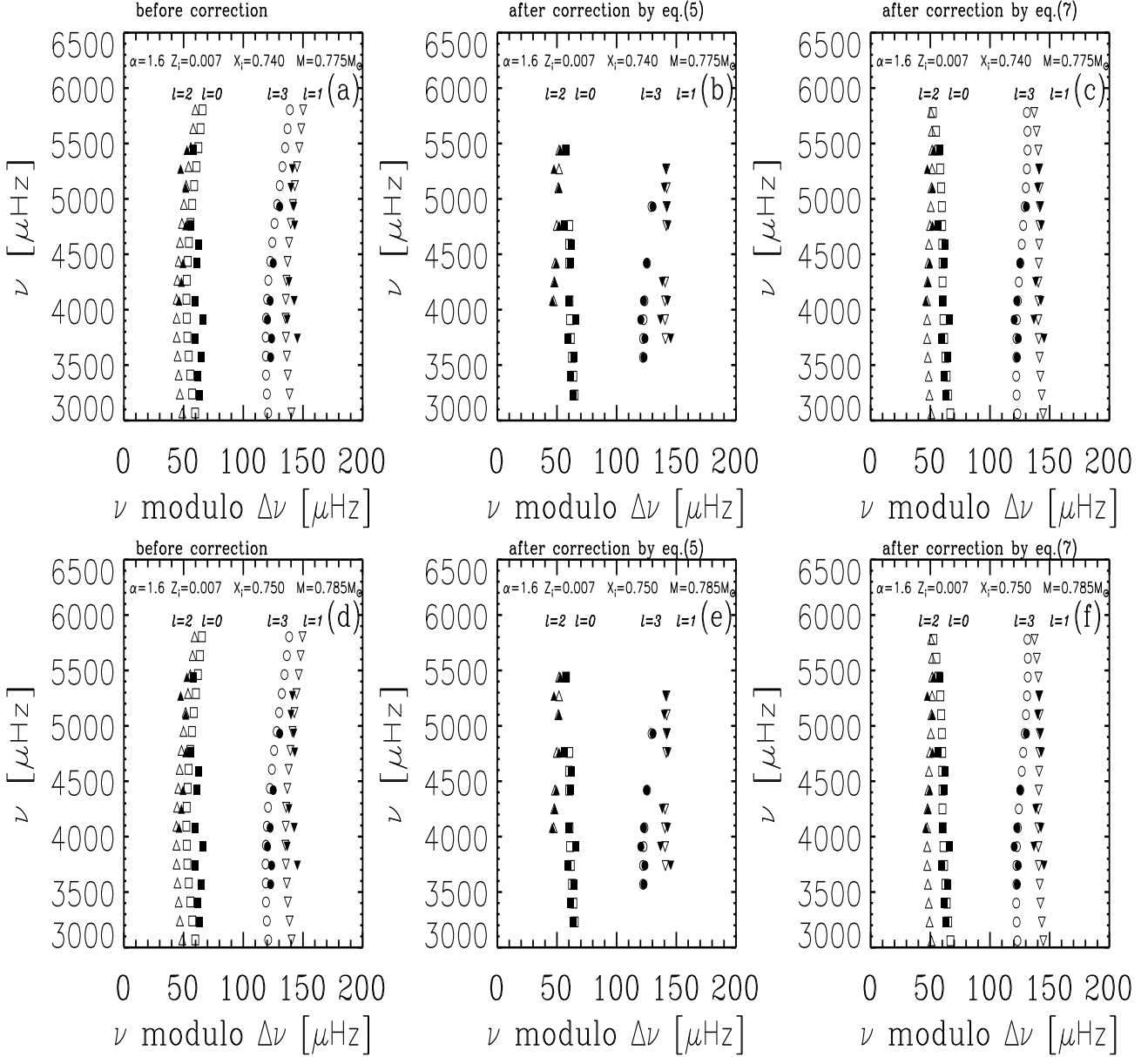


Fig. 4. Echelle diagrams for the optimal models M1 (upper panel) and M2 (lower panel). Left panel shows the case before applying near-surface corrections. Middle panel shows the case after applying near-surface corrections, according to Eq.(5). Right panel shows the case after applying near-surface corrections, according to Eq.(7). Open symbols refer to the theoretical frequencies, and filled symbols refer to the observable frequencies. Squares are used for $l = 0$ modes, diamonds for $l = 1$ modes, triangles for $l = 2$ modes, and circles for $l = 3$. The observable frequencies correspond to the average large separation about $170 \mu\text{Hz}$ (see text for details).

model parameters and characteristics of models M1 and M2 in Table 4.

5. Discussion and conclusions

Using the asteroseismic analysis and the empirical frequency correction for the near-surface offset presented by Kjeldsen et al. (2008) to correct our theoretical frequencies, we have derived the optimal model of τ Ceti and now list our main conclusions:

1. Using the latest asteroseismic observations, we have attempted to construct the optimal model of τ Ceti. We have only considered the models M1 and M2, which can closely describe the observations, as the optimal models. Furthermore, the model parameters of τ Ceti have been constrained to within narrow in-

tervals by the function $\chi_{\nu c}^2$, where the mass is in the range $M = 0.775 - 0.785 M_{\odot}$, the mixing length parameter in the range $\alpha = 1.6 - 1.8$, the initial metallicity in the range $Z_i = 0.0065 - 0.0075$, the initial hydrogen abundance in the range $X_i = 0.73 - 0.75$, and the age in the range $t = 8 - 10 \text{ Gyr}$.

2. We have found that the results of the non-asteroseismic observations (effective temperature and luminosity) inferred from spectroscopy are more accurate than those derived from interferometry for τ Ceti, because our optimal models are in the error boxes B and C derived from our spectroscopy results.

Acknowledgements. We are grateful to the anonymous referee for his/her constructive suggestions and valuable remarks that helped us to improve the manuscript. We also thank Professor Shaolan Bi and Dr Linghui Li for many useful comments and discussions. This work was supported by the support

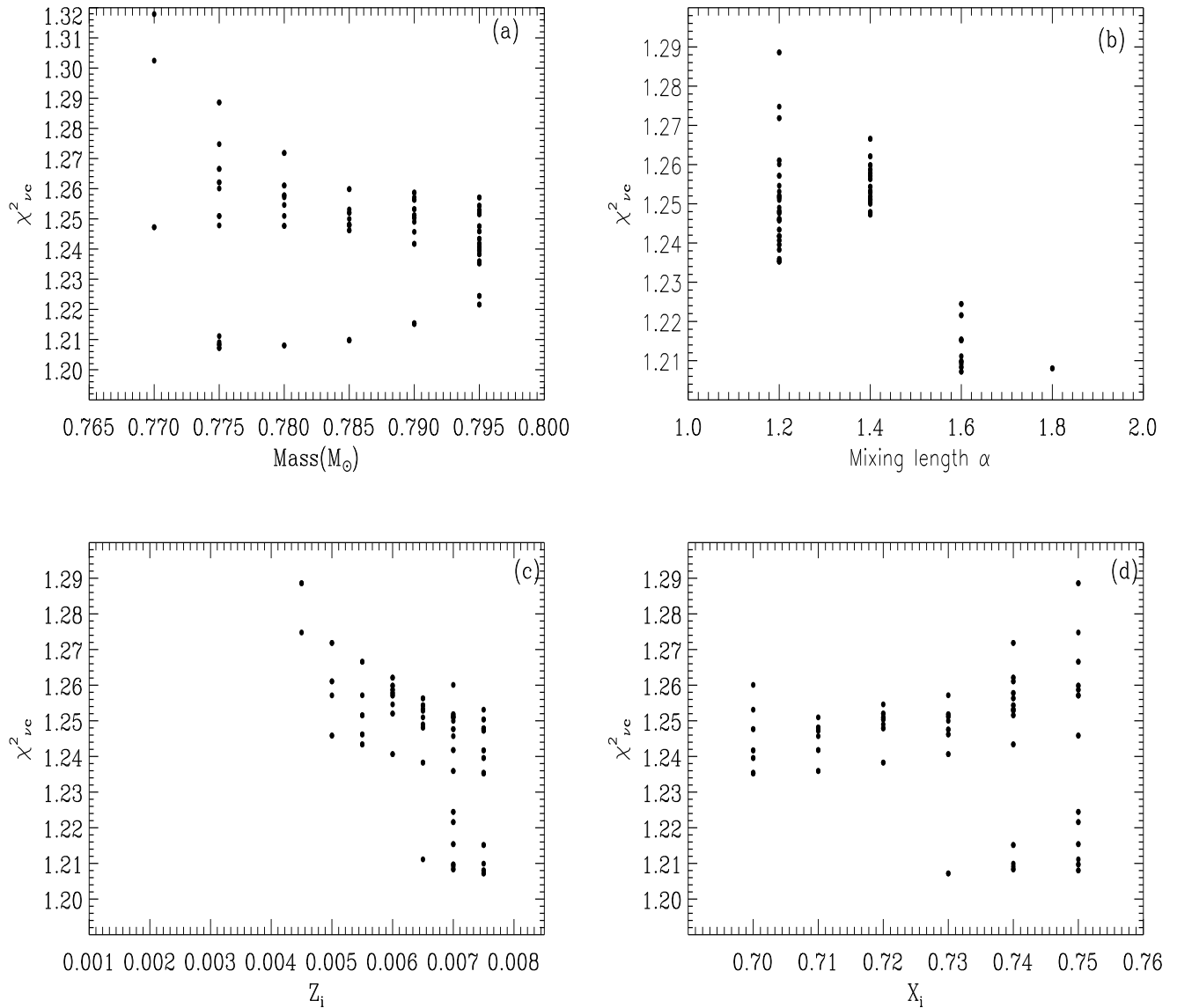


Fig. 5. (a). χ^2_{vc} values derived from Eq. (6), plotted as function of mass; (b). χ^2_{vc} values plotted as function of mixing length α ; (c). χ^2_{vc} values plotted as function of initial heavy element abundance Z_i ; (d). χ^2_{vc} values plotted as function of initial hydrogen abundance X_i .

of Shandong Nature Science Foundation (ZR2009AM021), Dezhou University Foundation(402811), and supported by The Ministry of Science and Technology of the Peoples Republic of China through grant 2007CB815406, and by NSFC grants 10773003, 10933002, and 10978010.

References

- Arentoft, T., Kjeldsen, H., Bedding, T. R., et al. 2008, *ApJ*, 687, 1080
 Angulo, C., Arnould, M., Rayet, M., et al. 1999, *Nucl. Phys. A.*, 656, 3
 Bessell, M. S., Castelli, F. & Plez, B. 1998, *A&A*, 333, 231
 Bedding, T. R., Butler, R. P., Kjeldsen, H., et al. 2001, *ApJ*, 549, L105
 Bedding, T. R., Kjeldsen, H., Butler, R.P., et al. 2004, *ApJ*, 614, 380
 Bedding, T. R., Butler, R. P., Carrier, F., et al. 2006, *ApJ*, 647, 558
 Bedding, T. R., Kjeldsen, H., Arentoft, T., et al. 2007, *ApJ*, 663, 1315
 Bedding, T. R., Kjeldsen, H., Campante, T. L., et al. 2010, *ApJ*, 713, 935
 Bouchy, F. & Carrier, F. 2002, *A&A*, 390, 205
 Bouchy, F., Bazot, M., Santos, N.C., Vauclair, S. & Sosnowska, D. 2005, *A&A*, 440, 609
 Bruntt, H., Bedding, T. R., Quirion, P. -O., et al. 2010, *MNRAS*, accepted
 Brown, T. M., Gilliland, R. L., Noyes, R. W., Ramsey, L. W. 1991, *A&A*, 368, 599
 Carrier, F., Bouchy, F., Kienzle, F., et al. 2001, *A&A* 378, 142
 Carrier, F. & Bourban, G. 2003a, *A&A*, 406, L23
 Carrier, F., Bouchy, F. & Eggenberger, P., 2003b. In: Thompson, M.J., Cunha, M.S., Monteiro, M.J.P.F.G. (Eds.), *Asteroseismology Across the HR Diagram*. Kluwer, p. P311.
 Carrier, F., Eggenberger, P., DAlessandro, A. & Weber, L., 2005a, *NewA*, 10, 315
 Carrier, F., Eggenberger, P. & Bouchy, F. 2005b, *A&A* 434, 1085
 Carrier, F. & Eggenberger, P. 2006, *A&A*, 450, 695
 Carrier, F., Kjeldsen, H., Bedding, T. R., et al. 2007, *A&A*, 470, 1059
 Carrier, F., Morel, T., Miglio, A., et al. 2010, *Ap&SS*, 328, 83
 Casagrande, L., Portinari, L. & Flynn, C. 2006, *MNRAS*, 373, 13
 Christensen-Dalsgaard, J. & Gough, D. O. 1980, *Nature*, 288, 544
 Christensen-Dalsgaard, J., Kjeldsen, H., Brown, T. M., et al. 2010, *ApJ*, 713, L164
 Chaplin, W. J., Appourchaux, T., Elsworth, Y., et al. 2010, *ApJ*, 713, L169
 De Ridder, J., Barban, C., Carrier, F., et al. 2006, *A&A*, 448, 689
 Di Folco, E., Thvenin, F., Kervella, P., et al. 2004, *A&A*, 426, 601
 Di Folco, E., Absil, O., Augereau, J.-C., et al. 2007, *A&A*, 475, 243

Table 3. The observational frequencies and the theoretical frequencies for model M1 & M2 before and after correction for near-surface offset, respectively.

| n | before | | | | correction | | | | after | | | |
|---------|---------------------------|---------|---------|---------|------------|----------|----------|----------|----------|----------|----------|----------|
| | Observational frequencies | | | | model | | | | model M2 | | | |
| $l = 0$ | $l = 1$ | $l = 2$ | $l = 3$ | $l = 0$ | $l = 1$ | $l = 2$ | $l = 3$ | $l = 0$ | $l = 1$ | $l = 2$ | $l = 3$ | |
| 18 | 3293.4 | ... | ... | ... | 3296.149 | 3377.700 | 3455.831 | 3529.092 | 3296.276 | 3377.775 | 3455.826 | 3529.043 |
| 19 | 3461.7 | ... | ... | 3692.9 | 3465.623 | 3547.268 | 3625.910 | 3699.994 | 3465.717 | 3547.304 | 3625.854 | 3699.900 |
| 20 | 3634.5 | ... | ... | 3863.7 | 3635.309 | 3717.485 | 3796.205 | 3870.802 | 3635.352 | 3717.479 | 3796.119 | 3870.664 |
| 21 | 3799.3 | 3885.3 | ... | 4030.3 | 3805.155 | 3887.715 | 3967.112 | 4042.136 | 3805.169 | 3887.661 | 3966.987 | 4041.970 |
| 22 | 3976.1 | 4046.8 | 4126.1 | 4202.5 | 3975.695 | 4058.363 | 4138.126 | 4213.984 | 3975.674 | 4058.279 | 4137.957 | 4213.769 |
| 23 | 4139.9 | 4222.7 | 4298.2 | ... | 4146.398 | 4229.665 | 4309.760 | 4385.981 | 4146.331 | 4229.535 | 4309.557 | 4385.721 |
| 24 | ... | 4388.3 | 4469.5 | 4545.1 | 4317.694 | 4401.101 | 4481.820 | 4558.582 | 4317.594 | 4400.922 | 4481.566 | 4558.284 |
| 25 | 4481.8 | ... | ... | ... | 4489.499 | 4573.112 | 4653.968 | 4731.322 | 4489.349 | 4572.896 | 4653.669 | 4730.972 |
| 26 | 4652.3 | ... | 4811.8 | ... | 4661.385 | 4745.381 | 4826.607 | 4904.208 | 4661.190 | 4745.115 | 4826.269 | 4903.817 |
| 27 | 4816.2 | 4903.1 | ... | 5060.5 | 4833.772 | 4917.748 | 4999.286 | 5077.435 | 4833.537 | 4917.439 | 4998.898 | 5077.001 |
| 28 | ... | 5072.3 | 5151.8 | ... | 5006.247 | 5090.515 | 5172.103 | 5250.549 | 5005.962 | 5090.165 | 5171.678 | 5250.071 |
| 29 | ... | 5240.0 | 5317.5 | ... | 5178.835 | 5263.220 | 5345.147 | 5423.822 | 5178.510 | 5262.825 | 5344.685 | 5423.311 |
| 30 | ... | 5411.2 | 5492.8 | ... | 5351.685 | 5436.051 | 5518.036 | 5597.086 | 5351.322 | 5435.623 | 5517.539 | 5596.541 |
| 31 | 5497.9 | ... | ... | ... | 5524.391 | 5608.945 | 5691.011 | 5770.097 | 5523.990 | 5608.485 | 5690.491 | 5769.528 |
| n | after | | | | correction | | | | model M2 | | | |
| $l = 0$ | $l = 1$ | $l = 2$ | $l = 3$ | $l = 0$ | $l = 1$ | $l = 2$ | $l = 3$ | $l = 0$ | $l = 1$ | $l = 2$ | $l = 3$ | |
| 18 | 3293.4 | ... | ... | ... | 3294.811 | 3373.293 | 3448.558 | 3521.990 | 3294.873 | 3373.414 | 3448.676 | 3522.028 |
| 19 | 3461.7 | ... | ... | 3692.9 | 3463.687 | 3542.188 | 3617.891 | 3692.166 | 3463.725 | 3542.282 | 3617.973 | 3692.180 |
| 20 | 3634.5 | ... | ... | 3863.7 | 3632.637 | 3711.616 | 3787.344 | 3862.157 | 3632.638 | 3711.682 | 3787.412 | 3862.151 |
| 21 | 3799.3 | 3885.3 | ... | 4030.3 | 3801.588 | 3880.925 | 3957.295 | 4032.565 | 3801.579 | 3880.961 | 3957.344 | 4032.561 |
| 22 | 3976.1 | 4046.8 | 4126.1 | 4202.5 | 3971.050 | 4050.500 | 4127.228 | 4203.364 | 3971.028 | 4050.527 | 4127.255 | 4203.345 |
| 23 | 4139.9 | 4222.7 | 4298.2 | ... | 4140.467 | 4220.554 | 4297.635 | 4374.174 | 4140.428 | 4220.560 | 4297.652 | 4374.152 |
| 24 | ... | 4388.3 | 4469.5 | 4545.1 | 4310.239 | 4390.548 | 4468.303 | 4545.430 | 4310.201 | 4390.534 | 4468.298 | 4545.417 |
| 25 | 4481.8 | ... | ... | ... | 4480.250 | 4560.894 | 4638.878 | 4716.651 | 4480.204 | 4560.877 | 4638.861 | 4716.641 |
| 26 | 4652.3 | ... | 4811.8 | ... | 4650.045 | 4731.252 | 4809.736 | 4887.824 | 4650.003 | 4731.224 | 4809.718 | 4887.837 |
| 27 | 4816.2 | 4903.1 | ... | 5060.5 | 4820.001 | 4901.433 | 4980.409 | 5059.120 | 4819.977 | 4901.408 | 4980.383 | 5059.162 |
| 28 | ... | 5072.3 | 5151.8 | ... | 4989.674 | 5071.706 | 5150.968 | 5230.066 | 4989.668 | 5071.692 | 5150.953 | 5230.148 |
| 29 | ... | 5240.0 | 5317.5 | ... | 5159.046 | 5241.582 | 5321.475 | 5400.908 | 5159.079 | 5241.584 | 5321.477 | 5401.051 |
| 30 | ... | 5411.2 | 5492.8 | ... | 5328.222 | 5411.212 | 5491.524 | 5571.452 | 5328.308 | 5411.249 | 5491.552 | 5571.669 |
| 31 | 5497.9 | ... | ... | ... | 5496.757 | 5580.498 | 5661.325 | 5741.433 | 5496.908 | 5580.579 | 5661.397 | 5741.746 |

Doğan, G., Brandão, I. M., Bedding, T. R., et al. 2009, *Ap&SS*, tmp..251D
Doğan, G., Bonanno, A. & Christensen-Dalsgaard, J. 2010, appear in the HELAS
IV International Conference proceedings in *Astronomische Nachrichten*
Demarque, P., Guenther, D. B., Li, L. H., et al. 2008, *Ap&SS*, 316, 31
Eggenberger, P., Carrier, F., Bouchy, F. & Blecha, A. 2004a, *A&A* 412, 247
Eggenberger, P., Charbonnel, C., Talon, S., et al. 2004b, *A&A*, 417, 235
Eggenberger, P., Carrier, F. & Bouchy, F. 2005, *NewA*, 10, 195
Eggenberger, P., Miglio, A., Carrier, F., et al. 2008, *A&A*, 482, 631
Ferguson, J. W., Alexander, D. R., Allard, F., et al. 2005, *ApJ*, 623, 585
Gai, N., Bi, S. L. & Tang, Y. K. 2008, *ChJAA*, 8, 591
Gray, D. F. & Baliunas, S. L. 1994, *ApJ*, 427, 1042-1047
Grevesse, N. & Sauval, A. J. 1998, *SSRv*, 85, 161
Guenther, D. B., Demarque, P., Kim, Y.-C., et al. 1992, *ApJ*, 387, 372
Guenther, D.B. 1994, *ApJ* 422, 400.
Guenther, D.B. & Demarque, P. 2000, *ApJ* 531, 503.
Iglesias, C. A., & Rogers, F. J. 1996, *ApJ*, 464, 943
Judge, P. G., Saar, S. H., Carlsson, M., Ayres, T. R. 2004, *ApJ*, 609, 392
Kallinger, T., Weiss, W. W., Barban, C., et al. 2010, *A&A*, 509, id.A77
Kervella, P., Thévenin, F., Morel, P., et al. 2004, *A&A*, 413, 251
Kjeldsen, H. & Bedding, T. R. 1995, *A&A*, 293, 87
Kjeldsen, H., Bedding, T.R., Baldry, I.K., et al. 2003, *AJ*, 126, 1483
Kjeldsen, H., Bedding, T.R., Butler, R.P., et al. 2005, *ApJ* 635, 1281
Kjeldsen, H., Bedding, T. R. & Christensen-Dalsgaard, J. 2008, *ApJ*, 683, L175
Li, L.H., Robinson, F.J., Demarque, P., Sofia, S. & Guenther, D.B. 2002, *ApJ*, 567, 1192
Miglio, A. & Montalbán, J. 2005, *A&A*, 441, 615
Miglio, A., Montalbán, J., Eggenberger, P., et al. 2009, *AIP Conference Proceedings*, Volume 1170, pp. 132-136
Miglio, A., Montalbán, J., Baudin, F., et al. 2009, *A&A*, 503, L21
Martić, M., Lebrun, J.-C., Appourchaux, T. & Korzennik, S.G. 2004a, *A&A*, 418, 295
Martić, M., Lebrun, J.C., Appourchaux, T., Schmitt, J. 2004b, In: Danesy, D. (Ed.), *SOHO 14/GONG 2004 Workshop, Helio- and Asteroseismology: Towards a Golden Future*, ESA SP-559, p. 563.
Metcalf, T. S., Creevey, O. L. & Christensen-Dalsgaard, J. 2009, *ApJ*, 699, 373

Metcalf, T. S., Judge, P. G., Basu, S., et al. 2010, *American Astronomical Society, AAS Meeting 215*, 424.16
Mosser, B., Bouchy, F., Catala, C., et al. 2005, *A&A*, 431, L13
Pijpers, F. P., Teixeira, T. C., Garcia, P. J., et al. 2003a, *A&A*, 406, L15
Pijpers, F. P. 2003b, *A&A*, 400, 241
Provost, J., Martić, M. & Berthomieu, G. 2004, *ESA SP* 559, 594.
Provost, J., Berthomieu, G., Martić, M. & Morel, P. 2006, *A&A* 460, 759
Rogers, F. J., & Nayfonov, A. 2002, *ApJ*, 576, 1064
Robinson, F.J., Demarque, P., Li, L. H., et al. 2003, *MNRAS* 340, 923.
Soubiran, C., Katz, D. & Cayrel, R. 1998, *A&AS*, 133, 221
Samadi, R., Georgobiani, D., Trampedach, R., et al. 2007, *A&A*, 463, 297
Stello, D., Chaplin, W. J., Basu, S., et al. 2010, *MNRAS*, 400, L80
Tang, Y. K., Bi, S. L., Gai, N., et al. 2008a, *ChJAA*, 8, 421
Tang, Y. K., Bi, S. L. & Gai, N. 2008b, *New Astronomy*, 13, 541
Tassoul, M. 1980, *ApJS*, 43, 469
Teixeira, T. C., Kjeldsen, H., Bedding, T. R., et al. 2009, *A&A*, 494, 237
Thévenin, F., Provost, J., Morel, P., et al. 2002, *A&A*, 392, 9
Thoul, A. A., Bahcall, J. N. & Loeb, A. 1994, *ApJ* 421, 828.

Table 4. Final model-fitting results for τ Ceti.

| Modelling parameters | model M1 | model M2 |
|-----------------------------------------------------|-----------|-----------|
| Mass M/M_{\odot} | 0.775 | 0.785 |
| Mixing length α | 1.6 | 1.6 |
| Z_i | 0.007 | 0.007 |
| X_i | 0.740 | 0.750 |
| Model characteristics | | |
| Effective temperature T_{eff} (K) | 5409 | 5387 |
| Luminosity L/L_{\odot} | 0.47985 | 0.47612 |
| Log(g) | 4.53187 | 4.53365 |
| Radius R/R_{\odot} | 0.78994 | 0.79339 |
| $(Z/X)_s$ | 0.00753 | 0.00749 |
| Age (Gyr) | 9.5 | 9.5 |
| $\langle \Delta\nu_0 \rangle$ (μHz) | 170.9222 | 170.9106 |
| $\langle \Delta\nu_1 \rangle$ (μHz) | 170.8621 | 170.8381 |
| $\langle \Delta\nu_2 \rangle$ (μHz) | 171.0555 | 171.0332 |
| $\langle \Delta\nu_3 \rangle$ (μHz) | 171.5120 | 171.4870 |
| $\langle \delta\nu_{02} \rangle$ (μHz) | 10.013 | 10.111 |
| $\langle \delta\nu_{13} \rangle$ (μHz) | 18.034 | 18.136 |
| Model corrected parameters | | |
| r_0 | 1.000302 | 1.000264 |
| r_1 | 0.9993002 | 0.9993007 |
| r_2 | 0.9984142 | 0.9984387 |
| r_3 | 0.9984967 | 0.9984996 |
| a_0 | -10.59438 | -10.32439 |
| a_1 | -8.270579 | -8.092409 |
| a_2 | -6.517972 | -6.377440 |
| a_3 | -5.891401 | -5.639216 |